NRC-CNRC
From Discovery to Innovation...
De la découverte à l'innovation...
La Science à l'œuvre pour le at work for Canada

NRC Publications Archive
Archives des publications du CNRC

Description of the Stereoscopic Particle Image Velocimetry System used by Memorial University of Newfoundland

Molyneux, W. D.

For the publisher's version, please access the DOI link below./ Pour consulter la version de l'éditeur, utilisez le lien DOI ci-dessous.

http://dx.doi.org/10.4224/8894892

NRC Publications Record / Notice d'Archives des publications de CNRC:
http://nparc.cisti-icist.nrc-cnrc.gc.ca/npsi/ctrl?action=rtdoc&an=8894892&lang=en
http://nparc.cisti-icist.nrc-cnrc.gc.ca/npsi/ctrl?action=rtdoc&an=8894892&lang=fr

Access and use of this website and the material on it are subject to the Terms and Conditions set forth at
http://nparc.cisti-icist.nrc-cnrc.gc.ca/npsi/jsp/nparc_cp.jsp?lang=en
READ THESE TERMS AND CONDITIONS CAREFULLY BEFORE USING THIS WEBSITE.

L'accès à ce site Web et l'utilisation de son contenu sont assujettis aux conditions présentées dans le site
http://nparc.cisti-icist.nrc-cnrc.gc.ca/npsi/jsp/nparc_cp.jsp?lang=fr
LISEZ CES CONDITIONS ATTENTIVEMENT AVANT D'UTILISER CE SITE WEB.

Contact us / Contactez nous: nparc.cisti@nrc-cnrc.gc.ca.

National Research Council Canada
Conseil national de recherches Canada
Canada

DOCUMENTATION PAGE

REPORT NUMBER	NRC REPORT NUMBER	DATE
TR-2006-12		May 2006
REPORT SECURITY CLASSIFICATION		**DISTRIBUTION**
Unclassified		Unlimited

TITLE

DESCRIPTION OF THE STEREOSCOPIC PARTICLE IMAGE VELOCIMETRY SYSTEM USED BY MEMORIAL UNIVERSITY OF NEWFOUNDLAND

AUTHOR(S)

David Molyneux

CORPORATE AUTHOR(S)/PERFORMING AGENCY(S)

Institute for Ocean Technology, National Research Council, St. John's, NL

PUBLICATION

SPONSORING AGENCY(S)

Institute for Ocean Technology, National Research Council, St. John's, NL

IOT PROJECT NUMBER	NRC FILE NUMBER		
42_2072_10			
KEY WORDS	**PAGES**	**FIGS.**	**TABLES**
PIV, Particle Image Velocimetry	iii, 35	19	10

SUMMARY

Particle Image Velocimetry (PIV) is an important technique for measuring velocities within a fluid. The flow through an illuminated plane (or volume) is seeded with small, reflective particles and a sequence of digital photographs is taken. By timing the intervals between photographs to ensure that the same particles are within the measurement space for each exposure, flow vectors can be calculated, once the measurement space has been calibrated. To calculate the velocity vectors, the total image is divided into smaller interrogation windows. The average particle movement within each interrogation window between two successive exposures is calculated. Velocity is determined by dividing the distance moved by the time interval between exposures. In its simplest form, the technique is applied in two dimensions using a single camera, but by using stereo photography, it can be extended to three dimensions. The main advantage of PIV over other measurement methods is that it can determine fluid velocity at all locations within the measurement plane simultaneously instead of having to make separate measurements at a series of different point locations. This is an important feature for analyzing unsteady flow.

ADDRESS National Research Council
Institute for Ocean Technology
Arctic Avenue, P. O. Box 12093
St. John's, NL A1B 3T5
Tel.: (709) 772-5185, Fax: (709) 772-2462

National Research Council Canada
Institute for Ocean Technology

Conseil national de recherches Canada
Institut des technologies océaniques

DESCRIPTION OF THE STEREOSCOPIC PARTICLE IMAGE VELOCIMETRY SYSTEM USED BY MEMORIAL UNIVERSITY OF NEWFOUNDLAND

TR-2006-12

David Molyneux

May 2006

TABLE OF CONTENTS

DESCRIPTION OF THE STEREOSCOPIC PARTICLE IMAGE VELOCIMETRY SYSTEM USED BY MEMORIAL UNIVERSITY OF NEWFOUNDLAND

INTRODUCTION

Particle Image Velocimetry (PIV) is an important technique for measuring velocities within a fluid. The flow through an illuminated plane (or volume) is seeded with small, reflective particles and a sequence of digital photographs is taken. By timing the intervals between photographs to ensure that the same particles are within the measurement space for each exposure, flow vectors can be calculated, once the measurement space has been calibrated. To calculate the velocity vectors, the total image is divided into smaller interrogation windows. The average particle movement within each interrogation window between two successive exposures is calculated. Velocity is determined by dividing the distance moved by the time interval between exposures. In its simplest form, the technique is applied in two dimensions using a single camera, but by using stereo photography, it can be extended to three dimensions. The main advantage of PIV over other measurement methods is that it can determine fluid velocity at all locations within the measurement plane simultaneously instead of having to make separate measurements at a series of different point locations. This is an important feature for analyzing unsteady flow.

The fundamental assumption in PIV analysis is that the calculated flow vectors follow a linear path based on the average seed particle displacement within a small area of the fluid. If there is a high degree of curvature to the flow, relative to the size of the interrogation window, the calculated particle traces will not match the real flow conditions. The PIV method will have difficulty in producing accurate results when there are large variations in the flow speed across the measurement area. In this situation, it is hard to determine the optimum time interval between the exposures. PIV analysis will be most accurate when using small interrogation windows and will be inaccurate for flow conditions where circulation occurs within an interrogation window.

The PIV system at Memorial University of Newfoundland was manufactured by LaVision GmbH of Goettingen, Germany and was purchased from LaVision Inc. of Ypsilanti, MI, USA. The system consisted of four main elements:

- Two Charge Coupled Device (CCD) cameras
- Twin-head Nd:YAG[1] laser and controller
- Computer for timing of laser and cameras and data acquisition

A photograph of the complete system, assembled in air, is shown in Figure 1.

[1] Neodium doped:Yttrium Aluminium Garnet

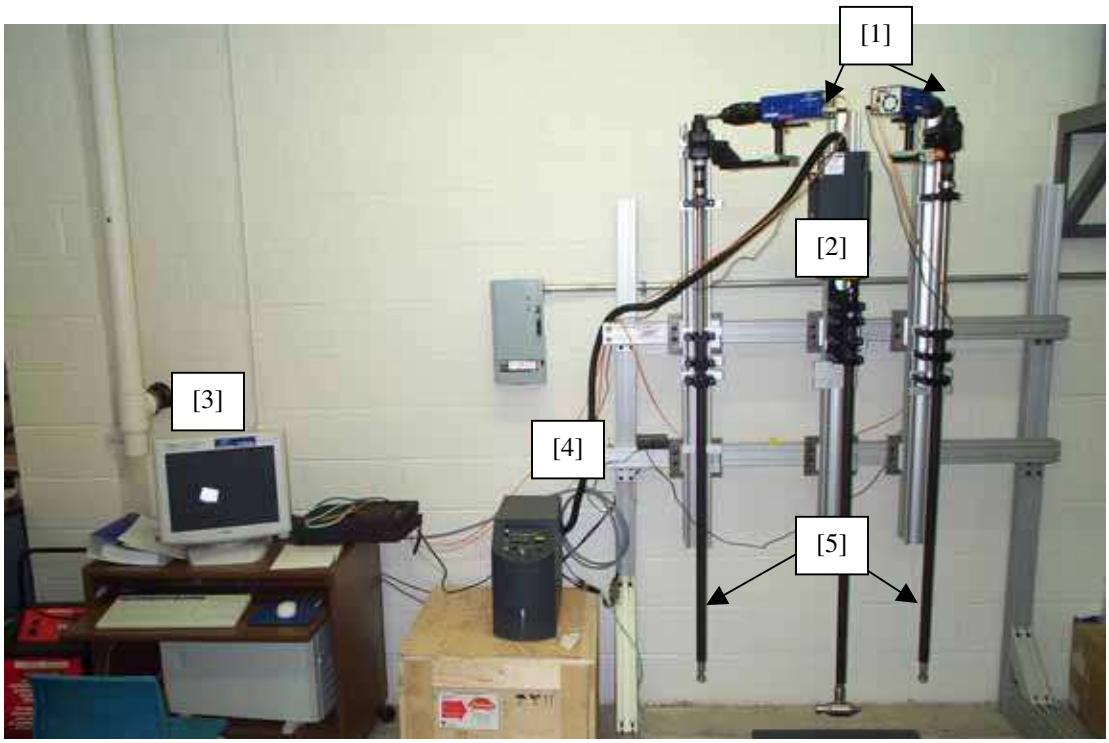

Figure 1, PIV System, view of complete system showing CCD cameras [1], laser head [2], computer [3], laser controller [4] and borescopes [5].

This PIV system was designed for the unique requirements of a ship model towing tank, where the operating fluid was water with a free surface. The unique features of this PIV system were the two borescopes. The cameras were mounted in air at the top of a borescope, which provided the capability for obtaining the underwater views. The advantage of this arrangement was that delicate cameras were kept well above the water surface, removing the need for expensive watertight housings. A similar arrangement was provided for the laser, but this was a plain tube, without the optics of a borescope.

There was some initial concern that the small aperture of the borescopes and the lenses inside the borescopes would result in the loss of too much laser energy and as a result photographs of the particles would be too dark. This was found not to be the case, provided that the underwater optics was cleaned daily.

Detailed descriptions of the component parts and analysis methods are given below (LaVision, 2002), together with a discussion on factors within the experiment and analysis procedures that affect the uncertainty of the results. Xu et al (2005) gave an overview description of the PIV system together with the results of some preliminary experiments.

SYSTEM COMPONENTS

Laser and Light Sheet Optics

The laser system used was a Solo 120 model supplied by New Wave Inc. This system consisted of a pair of Nd:YAG lasers with maximum energy output of 120 mJ/pulse and a maximum pulse repetition rate of 15 Hz. The pulsed laser beams were directed downwards through a stainless steel tube to a waterproof housing containing the light sheet optics. The light sheet optics consisted of a 45 degree mirror to turn the beam from vertical to horizontal and a fixed focal length cylindrical lens which controlled the divergence angle of the light sheet (lenses for 15° and 22.5° divergence angles were available). A second 45° mirror could be used to change the direction of the laser beam. With the second mirror removed, the laser shone directly out of the stern of the optical housing. With the second mirror in place, the beam was turned normal to the housing. Rotating the complete unit changed the direction of the beam.

At the top of the tube were two telescope lenses with infinitely adjustable focal lengths (between 400 mm and 2500 mm in water). These lenses were used to adjust the diameter of the laser beam, which in turn affected the thickness of the light sheet. These lenses were adjusted with the system assembled. The downstream side of the light sheet housing and connecting tube was fitted with a faired trailing edge to minimize wake turbulence.

Charged Couple Device Camera & Borescopes

Two identical Imager Intense™ cameras were used in the PIV system. Each camera had an adapter so that it could be used with standard Nikon C-mount or F-mount lenses. Specifications for the cameras are given in Table 1.

There was serial data transfer between the camera and the PCI-Interface-Board. A Programmable Time Unit (PTU) controlled the triggering of the camera and the synchronization with the laser. The exposure time of the camera, the laser power, and the interval between the two laser pulses were also adjusted by the PTU.

Parameter	Specification
Resolution (pixels)	1376*1040
Dynamic Range, Digitization	12 bits
Cooling	2-stage thermo electric
Quantum Efficiency	65% at 500 nm
Readout noise	4e
Readout Rate	16 MHz
Data Rate(Vector Fields/sec)	5Hz
Capture Sequence Capacity to RAM	2GB
Capture Sequence Duration to RAM	34 sec
Camera Interface	High Speed Serial, PCI bus

Table 1, Imager Intense Camera System Specification

The borescopes used in conjunction with the cameras were 1.9 m long. The collection cone angle of each borescope with no other optical devices was 35° (in air). At the lower end of each borescope was a prism, with a nominal collection angle of 20° (in air). In water the collection angle was reduced to 16° in width and 12° in height. The nominal viewing angle of each prism was normal to the borescope body but it could be changed within +/- 15° by adjusting the angle of the prism. Each borescope was fitted with a tapered fairing to minimize wake. Rotating the borescope about its centerline set the viewing direction.

Optimum Arrangement of CCD Cameras and Laser Light Sheet

The optimum arrangement of the PIV system is symmetrical, with one camera located on either side of the light sheet, as shown in Figure 1. This arrangement is most efficient in terms of spatial resolution because the distortion between the fields of view is the same for each camera. It is also relatively easy to maximize the overlap of the field of view for each camera to ensure the largest possible measurement space.

The optimum arrangement is not always possible in practice. An alternative arrangement is to have the two cameras are located on the same side of the light sheet. In this case, the field of view common to both cameras can be maximized, but the distortion is no longer symmetrical, and so spatial resolution is compromised slightly.

In two-dimensional PIV systems, the laser light sheet should be oriented with the strongest flow component and the camera image plane should be parallel to the light sheet. In practice this is not always possible and the camera may be at some angle to the light sheet. In this situation the depth of field becomes reduced, and only the centre of the image is in focus. This can be corrected by satisfying the Scheimpflug criterion, which requires the object plane, the lens and the image plane to intersect on a common axis. In practice, the lens is rotated relative to the image plane. The result is a constant depth of field over the complete image, but the image has increased perspective distortion. The Memorial PIV system cannot use the Scheimpflug criterion, because the lenses are directly fitted to the ends of the borescopes and rotating the lenses in this situation is not practical.

Calibration

Image distortion correction is an essential part of stereo PIV analysis because the image plane of the two cameras will always be at an angle to the object plane. In order to correct for the distortion between the two images a calibration procedure is carried out. For stereoscopic PIV this requires two planes, parallel to each other and a known distance apart, with marks at known locations on a grid that covers the complete field of view of each camera.

3D-PIV measurements require two different viewing angles of the same measurement space. The projected images of the 2-dimensional vectors on each plane are combined to give 3-dimensional vectors. Since the arrangement of both cameras is fixed it is possible

to calculate three velocity components from the two projections, by calibrating the measurement space against a matrix of points with known spacing in three dimensions.

The mapping function used for image distortion correction in the DaVis FlowMaster software is a third order two-dimensional polynomial function to map x_1 and y_1 in pixel coordinates within the image plane for camera one (including distortion) to corrected coordinates x and y in the object plane without distortion. The mapping function (for camera one at one z location) is of the form:

$$\begin{pmatrix} x_1 \\ y_1 \end{pmatrix} = \vec{f}\begin{pmatrix} x \\ y \end{pmatrix} = \begin{pmatrix} x + dx_1(x, y) \\ y + dy_1(x, y) \end{pmatrix}$$

With the normalized coordinates

$$s = \frac{2(x - x_0)}{nx}$$

$$t = \frac{2(y - y_0)}{ny}$$

defined by image size nx, ny (in pixels) with the origin (x_0, y_0) at the midpoint of the image. The values of dx_1 and dy_1 are given by

$$\begin{pmatrix} dx_1 \\ dy_1 \end{pmatrix} = \begin{pmatrix} a_0 + a_1 s + a_2 s^2 + a_3 s^3 + a_4 t + a_5 t^2 + a_6 t^3 + a_7 st + a_8 s^2 t + a_9 st^2 \\ b_0 + b_1 s + b_2 s^2 + b_3 s^3 + b_4 t + b_5 t^2 + b_6 t^3 + b_7 st + b_8 s^2 t + b_9 st^2 \end{pmatrix}$$

An additional set of coefficients is obtained for camera one at the second z location and two sets of coefficients for camera two at the same two z locations as camera one, for a total of four mapping functions. The calculation of the mapping functions requires at least 40 common grid points being visible in both camera images. For stereo PIV, the image distortion correction is applied to the vectors for each camera, calculated using the correlation function, rather than to the particle images.

The mapping functions are determined empirically using stereo images of a specially manufactured plate. The plate was machined so that each face is stepped with two parallel planes. Each plane has a matrix of white markers, evenly spaced at 22.5 mm. The thickness of the plate is 9mm and the step between the rows of dots on the plate is 2 mm. The advantage of this approach is that two parallel planes are accurately defined relative to each other. It is critically important that the calibration plate is located within the laser sheet and parallel to it, even though the calibration is carried out using visible light. Any rotation between the laser and the calibration plate will reduce the accuracy, since the vectors will be calculated in the reference frame of the calibration plate, not the frame of the light sheet.

For evaluation of the accuracy of the mapping function, the DaVis software calculates the size of the average deviation between the calculated position of the marks and the actual positions. The software manual (LaVision GmbH, 2002) states that a good calibration is considered to have an average error in the mapping function of less than 0.5 pixels and recommends that experiments should not be carried out if the average deviation is more than 2.0 pixels. The dialogue box also gives the dimensions of the 3-D image (in pixels), a chi squared statistic for the x and y directions, the number of marks used for calculating the mapping function and the average peak ratio (intensity) of the marks. The size of the image common to both cameras is greatest when the reference point is at the same pixel coordinate in both views, and the cameras are symmetrically located about the image plane.

Data Collection and Image Processing

Data collection and image processing was carried out with DaVis 7.1 software, supplied by LaVision Inc. This is a comprehensive software package that allows the user to manage all the optical aspects of carrying out a PIV experiment and analyzing the results.

Camera exposure times, the time between laser pulses and the number of frames used by the cameras were all set by the user, depending on the nature of the experiment. All of the experiments were carried out using stereo images, which required four exposures to produce the results. The four views were one from each camera at time t and one from each camera at $t+\delta t$. A series of frames were taken, which depended on the nature of the experiment. For simple flows, 20 exposures were used, but for more complex flows, 50 or 100 exposures were used.

The basis data product from each CCD camera is a pair of images of particles within the flow, separated by a time interval, δt. Each image represents a 2-dimensional projection of the seed particles within the illuminated plane. The first step is to analyze each image pair in the image plane of the camera. The total CCD image is divided into square interrogation windows (i.e. 128 x 128 pixels). A cross-correlation procedure is carried out to determine the correlation between pixel images in the first frame and the second frame.

The correlation function for one camera is of the form:

$$C(dx,dy) = \sum_{x=0,y=0}^{x<n,y<n} I_1(x,y) I_2(x+dx, y+dy), \frac{-n}{2} < dx, dy < \frac{n}{2}$$

I_1 and I_2 are the image intensities (grey scale) of the first and second interrogation windows, and the 2-dimensional array C gives the correlation strength for all integer pixel displacements (dx, dy) between the two interrogation windows. The size of the window is n x n pixels. This is also usually the size of the correlation plane, so that the maximum displacement calculated is $\pm n/2$. If a single pass analysis procedure is used, the interrogation windows have the same pixel coordinates in each frame.

The peak of the correlation function gives the most likely mean value of particle movement within the interrogation window (*dx,dy*). The position of the correlation peak can be identified to sub-pixel accuracy and the expected accuracy is between 0.1 and 0.5 pixels (LaVision GmbH, 2002). Individual peaks are determined from a three point Gaussian function. The actual resolution depends on the image quality, which is influenced by particle size, particle density and contrast. The correlation procedure is repeated for each interrogation window and for each camera, resulting in two sets of vectors (Vx_1, Vy_1) for camera 1 and (Vx_2, Vy_2) for camera 2.

Particles are excluded from the calculation if they flow out of the measurement space of either camera during the time interval δt. The particles can move out of the in-plane interrogation window, or if the flow is three-dimensional, they can flow out through the plane of the light sheet. The value of δt to minimize the loss of seed particles from within the laser sheet depends on the local flow velocity components for the experiment and must be adjusted accordingly. The reliability of vector calculations will be increased considerably by aligning the laser so that the weakest flow component is through the plane of the laser.

The required vector is (*Vx, Vy, Vz*) relative to the plane of the light sheet. The set of equations determined from the two cameras is over specified in that there are four variables available to solve for three unknown quantities. This feature can be used to improve the accuracy of the PIV measurement by providing an additional check on vector accuracy. The linear equation system is solved by the normal equation and the remaindered degree of freedom error should be small (<3 pixels), which provides a criterion for removing spurious vectors.

The size of the interrogation window must be decided a priori or by trial and error. If trial and error is used, the interrogation window sizes used in the analysis are reduced until there is no significant change in the calculated flow patterns.

The basic image analysis procedure described above can be refined to increase the signal to noise ratio. Initially, the division of the pixel image of the seed particles into interrogation windows was based on the geometry of the window and not the flow pattern. Particles close to the downstream edge of an interrogation window at the first exposure may have moved out of that window in the second exposure, and new particles will have flowed in. As a result, the number of particles common to both views is reduced.

Using one of the following techniques can increase the number of particles included in the analysis:

- Overlap windows: The second interrogation window includes an overlap with neighbouring windows, based on a fixed fraction of the original grid.

- Adaptive Multiple passes
    - Fixed window size: Uses vectors calculated in first iteration to move the second interrogation window off the initial grid.

    - Reduced window size: For the second iteration, the window size is half the initial size, and the shift relative to the original window is calculated based on the mean vector calculated in the first pass.

The origin for starting the analysis of the PIV images is the top left-hand corner of the CCD image. If a fixed window size is used, there may be parts of the image that are not processed (bottom and right side) if the full image dimension is not an integer number of interrogation windows.

Once the flow vectors have been computed for an equidistant grid, further processing can be carried out to improve the quality of the image by removing spurious vectors. These include:

1. Allowable vector range
The calculated vectors are filtered on the basis of allowable ranges (in pixel or m/s). The range is specified based on a mean value, with upper and lower limits (which are the same).

2. Peak ratio
The peak ratio factor Q, compares the magnitudes of the highest peak in the correlation coefficient matrix relative to the noise and the second highest peak relative to the noise, based on the function

$$Q = \frac{P_1 - \min}{P_2 - \min}$$

where P_1 is the highest value in the correlation matrix, P_2 is the second highest peak, and min is the lowest value. For Q=1.5 or higher, the main peak is well defined and probably represents a valid vector. Peak ratios close to 1.0 most likely represent invalid vectors and should be removed.

3. Median filter
In this case, the analysis is based on a three by three grid of interrogation windows, and the vector in the centre square is compared to the values in the other eight squares. The centre vector is rejected if it is outside the range given by the median vector of the eight neighbours, plus or minus a deviation based on a multiple of the RMS of the neighbouring vectors. Another criterion for filtering includes removing the vector if there are less than a set number of neighbouring cells with calculated vectors.

In some cases, the background to the particle image may not be a constant intensity. This is most likely to occur in regions of the image close to the solid boundary of a model, where the laser light is reflected. To improve particle images in these situations, a filter, similar to a high pass filter, can be used. The aim is to make the background more uniform and increase the contrast between the particles and the background. To obtain this condition, a scale parameter is used, which must be at least twice the mean particle diameter in pixels. An alternative is to subtract a constant value. The disadvantage of this technique is that some information is being removed from the image, and the user must be sure that the information being removed is less important than the information being retained.

Once the most suitable analysis procedure has been developed for a particular experiment, based on a single frame using interactive methods, the image processing and vector analysis can then be carried out for all frames in a sequence using batch processing. For steady flows, sets of vectors can be combined to provide an average vector map over a period of time.

The results can be visualized in a variety of ways. Particle images and calculated vectors can be viewed as movies, so that particle movement and calculated vectors can be inspected. Vector maps of the flow can be plotted, and summary statistics of the images (particles or vectors) can be calculated.

Effect of Seeding on Accuracy of PIV Measurements

Successful seeding of the flow is a key factor in obtaining reliable results from PIV experiments. The seed particles should be neutrally buoyant in the test fluid, so that there are no velocity components occurring due to gravity or buoyancy forces. Also, the particles should be small in relation to the flow patterns, so that the particles follow the local movement of the fluid, not the motion due to average fluid forces acting on the particle.

It is desirable to have particle diameters viewed at the CCD between two and three pixels. The DaVis software uses a three-point Gaussian peak approximation on the measured intensities to identify the centre of a seed particle to sub-pixel accuracy. If the image size is less than one pixel, there is a tendency for the calculated vectors to be integer numbers of pixels and resolution of the vector field is compromised.

The accuracy of the vector calculation within a given interrogation window increases with the number of particle image pairs included in the correlation calculation. In practice three or four particle image pairs in each interrogation window are sufficient for accurate definition of the correlation peak. Increasing seed density allows the size of the interrogation window to be reduced, with the result that the spatial resolution of the flow can be increased. The upper limit of seeding concentration is that there must be a clear contrast between particles and the background

The final factor to consider in determining the accuracy of PIV measurements is the number of images of the same nominal flow condition. The accuracy of steady flow conditions can be improved if the vectors are based on the average value from multiple image pairs. The number of frames used to determine this will depend on factors such as the degree of spatial resolution required and the length of time available for the experiment.

PREVIOUS APPROACHES TO ESTIMATING UNCERTAINTY IN STEREOSCOPIC PIV EXPERIMENTS

Uncertainty in stereoscopic PIV systems has been discussed in the literature, but the focus has been on the accuracy of the mapping function and the vector reconstruction. The theoretical errors in the vector reconstruction from stereo images have been determined (Lawson and Wu, 1997a). The uncertainty in translational systems (with no Scheimpflug correction) and rotational systems (with Scheimpflug correction) were determined. The focus of the analysis was on determining the relative error between the in-plane vectors (x, y) and the through plane vectors (z) and results were presented in the form of an error ratio, rather than an absolute value. The objective was to determine the arrangement of the PIV system with the minimum uncertainty in the z direction, relative to the x-y plane.

To carry out this analysis Lawson and Wu (1997a) assumed that the uncertainty in the vectors determined at the object plane (x, y, z) was represented by an RMS value and that this value was equal in each direction. Then, by considering the geometry (distances between cameras and viewing angles) and the magnification of the PIV system, the error ratio (uncertainty) based on the geometric reconstruction was calculated. The error ratio was mapped over the complete object plane.

Lawson and Wu's analysis showed that at the centre of the lens, the two systems produced very similar ratios, but as the distance off the centre was increased, the error ratios for the rotational system were up to 40% lower than the for the translational system. This analysis did not consider any errors due to distortion correction.

The same authors carried out an uncertainty analysis of a complete stereoscopic PIV system in another paper (Lawson and Wu, 1997b). This was an experimental approach to uncertainty analysis, starting with determination of the 3-D mapping function, using a calibration plate. A test PIV specimen was constructed by suspending seed particles in epoxy resin. The advantage of this approach was that it used real seed particles, but fixed them relative to each other. When the block was moved all particles were moved a constant distance and the resulting vectors calculated by the PIV software should be constant across the whole field of view for each camera. The test specimens were illuminated using laser light, and images collected. The specimen was then moved known distances ($\delta x, \delta y, \delta z$) and the distances calculated by the PIV system were compared to the known distances. Different viewing angles between 10 and 45 degrees were

evaluated, but the cameras were always on the same side of the light sheet, and at the same viewing angle relative to the light sheet.

Lawson and Wu (1997b) conclude that optimum performance will be obtained by using viewing angles between 20 and 30 degrees for camera *f* numbers of *f*16 and higher. The uncertainty analysis for uniform flow gives RMS errors of 1-2% for the in-plane flows and 3-4% for the through plane flow (which was within the range of 8% to 18% of the theoretical error). These values were for cases where particle movement was restricted to between 15% and 30% of the interrogation window dimension. Below this displacement range, the system did not have enough resolution.

Other researchers have used variations on the basic approach taken by Lawson and Wu. Soloff et al (1997) investigated the robustness of a 3-dimensional mapping function for stereoscopic PIV analysis. They used an aluminium calibration plate with a 9 by 9 grid of holes, 0.5mm diameter at 27mm intervals. The plate was lit from behind. The calibration procedure was to take images of the plate at three z locations of 0, +/-0.5 +/-0.005mm. This gave rms errors in the mapping function of 1.1 pixels for camera 1 and 1.2 pixels for camera 2. This translated to 0.045mm and 0.051 mm respectively.

After the calibration, images of the plate were taken with each camera, and then the plate was moved small but known distances in y and z directions, and images of the plate at the new location were taken. Cross correlation was used to analyze the image pairs from each camera. The two-dimensional vector fields for each camera were filtered and then stereoscopically combined to obtain the three-dimensional vectors (*x, y, z*) calculated from the PIV software.

The errors between the calculated vectors and the known movement of the calibration plate (in each direction) were plotted as contours of error against the x and y coordinates for the measurement space. The results were contours of error, spatially distributed over the measurement area.

The estimated error (based on the highest contour shown, which looks to be about 95% of all measurements) for each axis was

x +/-0.0050 mm
y +/-0.0036 mm
z +/-0.0200 mm

Resulting errors were not evenly distributed over the measurement space, and it would have been useful to see an overall statistical distribution of the errors. The error in the results was the same order of magnitude as the error calculated from the mapping function for each camera during the calibration, so in this case the mapping function is the primary source of the error.

Calcagno et al. (2002) discussed the uncertainty of a stereoscopic PIV system designed to measure flow in the wake of a model propeller behind a ship. The facility used for

conducting these experiments was a cavitation tunnel. An underwater camera was aligned directly behind model to measure flow in the plane of the propeller. The second camera, mounted outside the cavitation tunnel had a viewing angle between 36 and 40 degrees off the centreline of the model.

For the camera looking directly at the in-plane vectors, the mapping function had an estimated particle resolution within 0.1 pixels (4 cm/s for the flow conditions considered). This view was treated as a two dimensional view, with minimal distortion. Error in the through plane measurements was thought to come from the stereo reconstruction (mapping function). This was analyzed using a target consisting of a 'typical' PIV image, which was moved a known distance (1mm) along the normal axis. The calculated uncertainties were under 2.5% in the 'in-plane' displacements and under 3% in the through plane displacements. The authors discuss the fact that the errors may be optimistic, since they were obtained from a bench test, without the model or the rotating propeller.

UNCERTAINTY ANALYSIS FOR MEMORIAL UNIVERSITY'S PIV SYSTEM

A detailed uncertainty analysis for the PIV measurement geometry, such as the one described by Lawson and Wu (1997) was not carried out for the PIV system. The facility schedule did not allow enough time to carry this out in situ. The uncertainty was estimated from the combination of the errors in the mapping function reported by the DaVis 7.1 software, and some special experiments to measure undisturbed flow.

Preliminary experiments to measure flow patterns around a ship model in a towing tank (Molyneux & Xu, 2005) showed that it was necessary to have a seeding system to inject the seed particles into the flow. Without a seeding system, there was insufficient particle concentration to obtain consistent measurements. One of the main concerns with this approach was the effect of the seeding system on the flow. Some experiments were designed to determine this effect, and these were combined with the uncertainty analysis.

The PIV measurements to study the flow patterns created by the seeding rake were carried out in the Ice Tank of the National Research Council's Institute for Ocean Technology. The ice tank is 80 m long, 12 m wide and 3 m deep. The tank is equipped with a large towing carriage, which is fitted with an adjustable test frame. The whole frame can be adjusted vertically and the as two longitudinal beams that can be moved independently. Each beam has a measurement scale relative to the centreline of the carriage, so the exact position of the beam is known. The PIV equipment was fitted to the beam on the south side of the carriage.

A temporary frame for the PIV system was built around the test beam, using extruded aluminium sections. The laser was oriented normal to the direction of motion, so that the measurement plane was across the direction of motion for the undisturbed flow. The borescopes for the CCD cameras were mounted symmetrically, approximately 650mm

either side of the laser sheet. Camera 1 was at the forward end of the carriage, and Camera 2 was at the aft end. The centre of the measurement window was approximately 950 mm away from the underwater optical unit for the laser. The PIV system is shown fitted to the towing carriage in Figure 2.

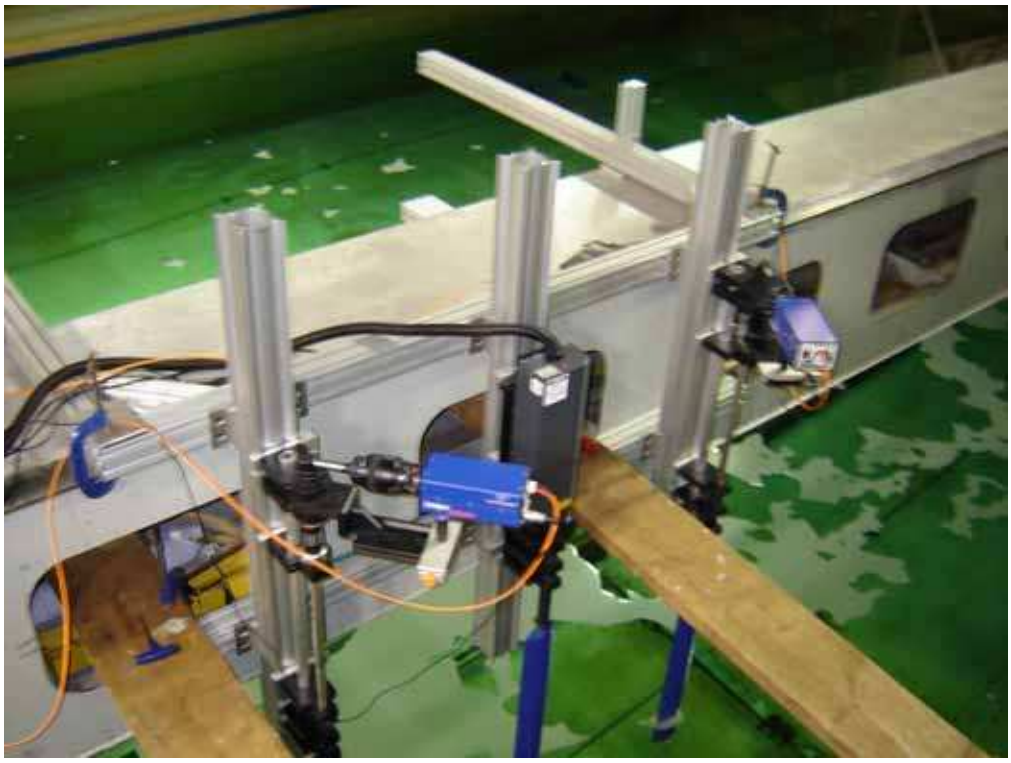

Figure 2, PIV system fitted to towing carriage

In-situ calibration of the measurement space was carried out prior to testing. A Type 30 calibration plate, supplied by LaVision GmbH, was used. The plate was 300mm by 300 mm square. The plate was suspended within the laser plane. The views from each camera were checked to ensure that the field of view was approximately the same. The calibration was carried out using visible light, following the procedures described in the DaVis 7.1 software (LaVision, 2005).

The image taken from Cameras 1 and 2 during the calibration, together with the calculated mapping functions are shown in Figures 3 and 4. The combined image, after correction for the distortion is shown in Figure 5. This image is the calculated view normal to the plane of the calibration plate, whereas the raw images from the cameras include the perspective distortion.

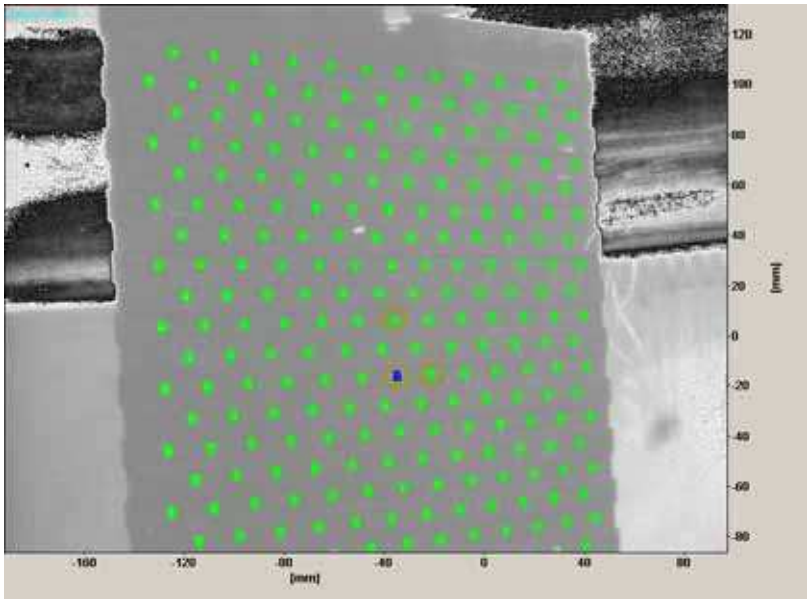

Figure 3, Image from Camera 1 showing points used in calculating mapping function

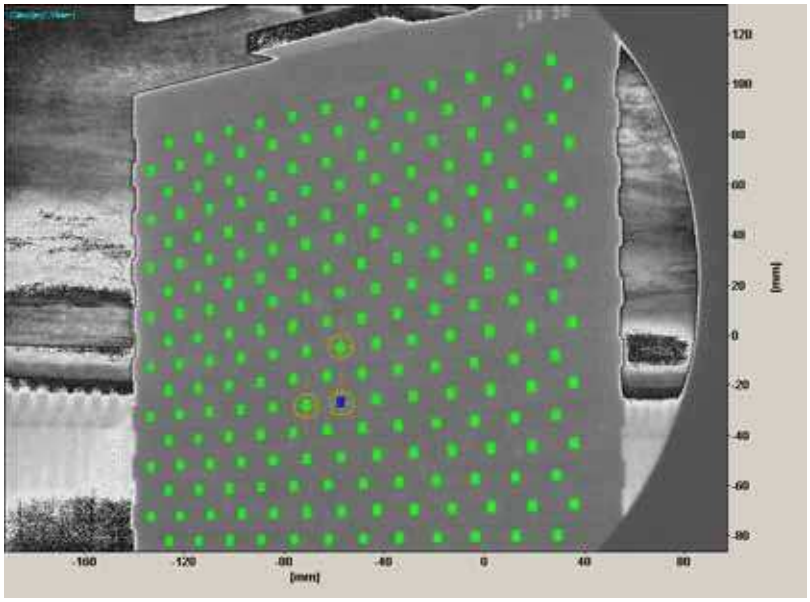

Figure 4, Image from Camera 2 showing points used in calculating mapping function

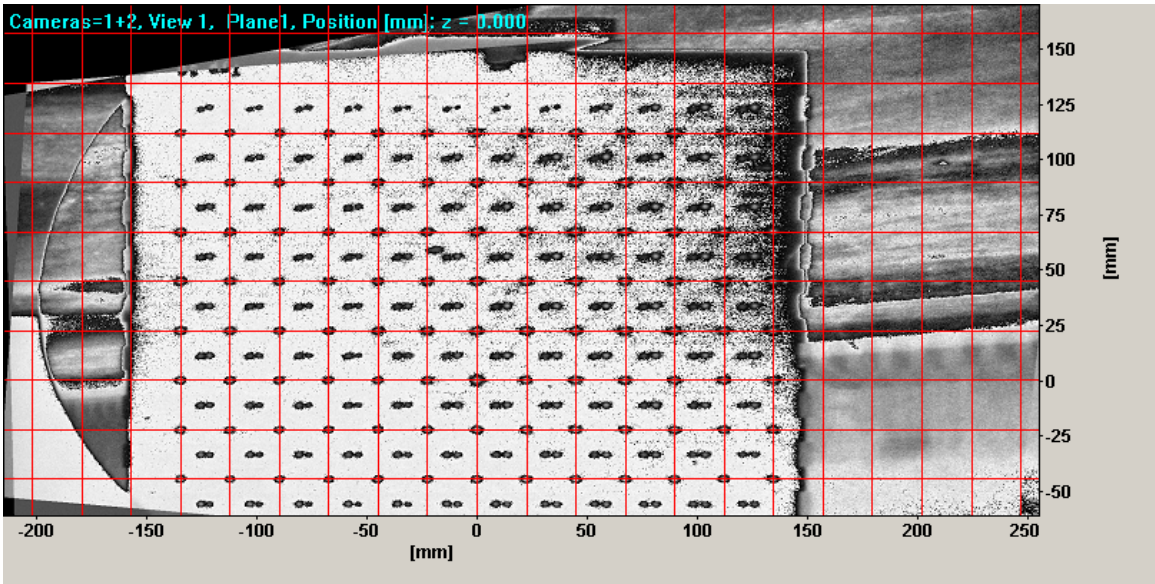

Figure 5, Corrected image, showing extrapolation over full image

A summary of the fit of the mapping function to the known distance between the points on the calibration plate is given in Table 2.

	Camera 1	Camera 2
RMS deviation, pixel	0.141390	0.173760

Table 2, Fit to mapping functions

The final corrected image had the dimensions given in Table 3.

	pixel	mm	Pixel/mm
X dimension	2250	463.811	4.851
Y dimension	1110	333.995	3.323
Average			4.087

Table 3, Final image size, corrected image

δt, microsec	δt, sec	95% CI, mm	95% CI, m/s
500	0.0005	0.083325	0.166649
700	0.0007	0.083325	0.119035
800	0.0008	0.083325	0.104156
1000	0.001	0.083325	0.083325

Table 4, 95% Confidence Intervals for calculated speeds, based on uncertainty in mapping function.

Assuming that the residuals in the polynomial fit to the mapping function follow a normal distribution, then the confidence intervals for the calculated speeds can be calculated for different laser timing intervals. The resulting calculations are given in Table 4, for the range of time intervals between first and second exposures, used in the free stream experiments.

The calculated uncertainties are relatively high compared to the published uncertainty analyses discussed above. The calculated RMS deviation of the mapping function, in pixels, is very good when compared to the previously published results (Soloff et al, 1997), which determines RMS errors to within 1 to 1.1 pixels. Soloff's results however translated into much smaller spatial errors of 0.05mm, since the measurement area was much smaller.

Smaller measurement areas are more common in previously published PIV research on ship models. A study of ship wake using PIV in a large circulating water tunnel (Di Felice and De Gregorio, 2000) used a measurement window of 18,000 mm^2. Gui et al (2001) presented wake data for a ship model using a measurement window of 5,625 mm^2. Calcagno et al (2002) used the largest measurement area of 50,000 mm^2 for measuring the downstream wake in the race of a working propeller behind a ship model. This large window size captured all the important features of the flow in a single window. The measurement window for the MUN PIV system used in this study was 155,000 mm^2, which is over three times the size of the next largest. Test particle images showed that the average particle diameter was between 2 and 3 pixels, so data collected using the large window should not be subject to bias caused by peak locking. Since the flow conditions were expected to be unsteady, the largest possible measurement window was desirable.

Table 4 gives the effect of the time between the laser pulses on the uncertainty in the resulting speed measurement. When the PIV measurement plane is oriented across the flow, it is necessary to use short time intervals between the laser pulses, otherwise particles have moved through the laser sheet, and no data is obtained. With this orientation, it is necessary to accept higher uncertainty than for an orientation along the flow, where there is more possibility for variation in the timing of the pulses.

The analysis described here makes no allowance for the errors in separate velocity components. The more detailed analysis of stereo PIV carried out by other researchers suggests that the through plane measurements are generally less accurate than the in-plane measurements. Theoretical error analysis carried out for stereoscopic PIV systems in similar configurations to the one described here (Lawson and Wu, 1997), suggests a range of uncertainty between 8% and 18%. At 1 m/s, the calculated uncertainties for pulse intervals between 500 and 1000 μs are within that range.

SEEDING DELIVERY SYSTEM

Seeding the flow is an essential element of PIV measurements. If the PIV system is stationary and the fluid is stationary, then it is only necessary to seed the volume of fluid close to the laser sheet. This option is feasible for a stationary PIV system in a towing tank, where the ship model passes through the measurement volume. The movement of the model ship through the seeded fluid will cause a disturbance and the movement of the seed particles can be observed. The disadvantage of this system is that very little data is obtained at a specific location on the hull, since only one set of frames is obtained for each run down the tank.

If the fluid is moving relative to the PIV system then one option is for the complete volume of the fluid to be seeded. This option is feasible for a circulating water tunnel, where particles can be kept in circulation by the moving fluid. This is not a practical option in a towing tank, which has a very large volume of stationary fluid. Eventually almost all of the seed particles will either sink to the bottom or float to the top requiring the fluid to be re-seeded after a certain period of time.

A practical alternative is to introduce particles to the flow so that seeding is present only in the measurement volume for the duration of the measurements. This should allow for a controlled use of the seeding particles, and should provide high quality PIV images, since the seeding density is correct for the volume of fluid being studied, and the parts of the flow that are of no interest to the study are ignored. The disadvantage of this approach is that the seeding delivery system may affect the momentum of the seeding particles, which will influence the results.

PROTO-TYPE SEEDING DELIVERY SYSTEM

Since there was very limited experience at Memorial University with seeding systems for PIV, it was decided to make the initial system as cheaply as possible, so that it would be a small expense if it had to be scrapped completely. A sketch of the initial concept is shown in Figure 6.

The prototype system was constructed from readily available plumbing parts and included:

- Holding tank and drain (plastic laundry tub)
- Dishwasher connectors and pipes
- Tap to control flow rate
- Seeding rake made from 22.2 mm ($^{7}/_{8}$ inches) diameter copper pipe and plumbing connectors

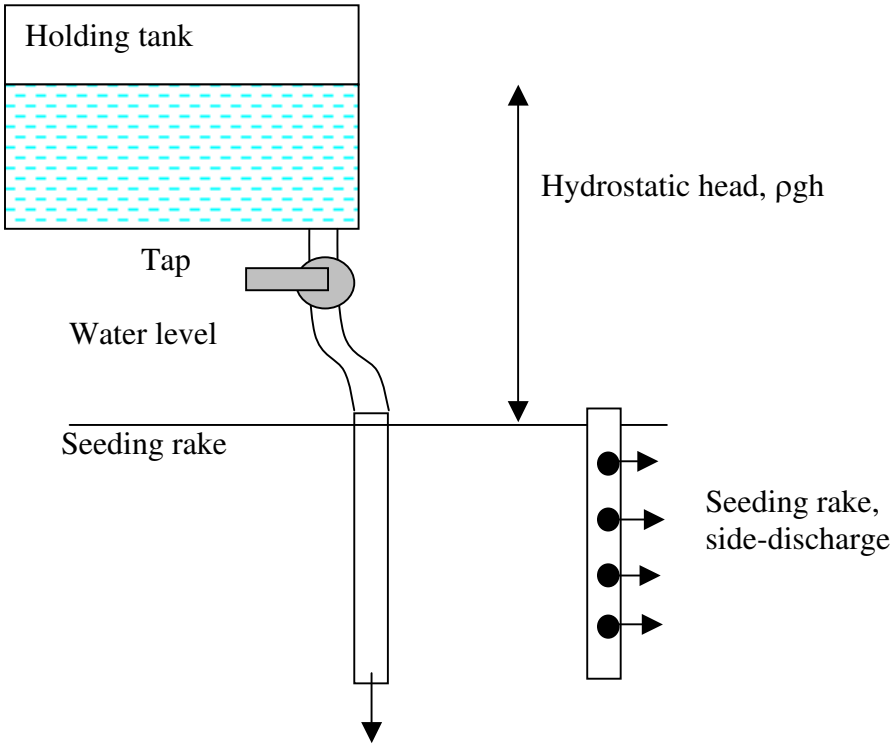

Figure 6, Concept sketch for seeding delivery systems

The system used hydrostatic pressure to deliver the seeded flow from the holding tank to the measurement volume. Adjusting the height of the holding tank, relative to the water level, controlled the static head and a tap was used to control flow rate. Water in the holding tank was taken from the local mains supply. The seeding particles were added and the mixture was stirred prior to carrying out an experiment, to keep the seeding evenly distributed.

Two arrangements of discharge holes were evaluated. The end-discharge system was intended to seed the flow upstream and above the area of interest for the flow measurements, as shown in Figure 7a). Since the rake was nominally above the measurement area, the disturbance to the flow caused by the rake over the measurement area was minimized. The side-discharge system was also placed upstream of the required measurement area but the seeded fluid was discharged from the downstream side of the pipe, as shown in Figure 7b). The potential disadvantage of this approach was that the rake was close to the path of fluid entering the measurement area, and the wake of the seeding rake may effect the measurements.

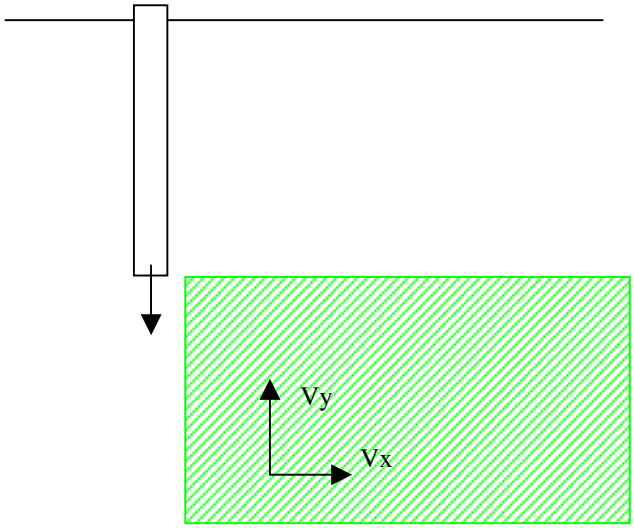

Figure 7a) Measurement area for end discharge rake and velocity components

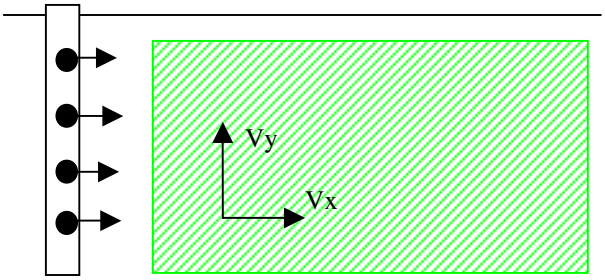

Figure 7b) Measurement area for side discharge rake and velocity components

Two versions of the side-discharge seeding rake were made. The first version had holes 6.35 mm ($^1/_4$ inches) diameter drilled at 41.3 mm ($1^5/_8$ inches) spacing and the second version had holes 1.58 mm ($^1/_{16}$ inches) diameter drilled at 19.1 mm ($^3/_4$ inches) spacing. The version with small holes worked well at zero velocity, but did not deliver sufficient seeding particles at the forward speeds required for ship model work (0.1m/s and above). The seeding rakes are shown in Figure 8.

Figure 8, Prototype seeding rakes (rake with large diameter holes on right)

Seeding Particles

The seeding particles used for all the experiments were hollow, silver coated spheres (SH400S33) supplied by Potters Industries of Valley Forge PA, USA. Preliminary experiments on different types of seeding powder (Molyneux & Xu, 2005) indicated, that although these were the most expensive in terms of unit price, the image quality and the ability of the particles to stay suspended for the longest time make them the most viable technical solution. A significant advantage of the silver coating was that it was highly reflective to laser light and the particles appeared bigger than actual size when viewed in the CCD camera. The particle specifications are given in Table 5 (Potters Industries, 2005).

Particle composition	Silver coated glass
Shape	Spherical
%Ag metal	33
Ten percentile, particle diameter, microns	8
Ninety percentile, particle diameter, microns	20
Mean particle diameter, microns	14
True density, g/cc	1.7

Table 5, Seeding particle specifications

No formal method for ensuring constant seeding concentration was developed for these experiments. The holding tank was filled to approximately the same level each time and seeding particles were added by scoops with a small spoon. Visually, the mixture was opaque and cloudy grey in colour. The analysis software was tolerant to a range of particle concentrations within the required minimum of three or four vector pairs and the

practical maximum of sufficient contrast between particles and background. As a result, it was not critical to keep seeding concentration tightly controlled.

EXPERIMENTS WITH PROTO-TYPE SEEDING DELIVERY SYSTEM

Experiments with the prototype seeding system were carried out in the Ocean Engineering Research Centre towing tank (Molyneux and Xu, 2005). The measurement plane for these preliminary experiments was to have the laser parallel to the direction of motion for the carriage, so that the strongest flow direction was in the plane of the measurement. Data was collected and analyzed using DaVis 6.2.3, which was the software originally supplied with the PIV system in January 2004. DaVis 7.1 was not available at the time the preliminary experiments were carried out.

Measurements of flow vectors for carriage speeds of 0.10, 0.30, 0.50, 0.75 and 1.00 m/s were made using the PIV system. Some experiments were carried out with particles introduced to the flow using the seeding systems described above and some were carried out using only particles left in the fluid from previous runs. When the seeding system was used, it was located upstream of the measurement area, just out of the field of view for the cameras. For the side discharge version, the rake extended across the depth of the field of view. For the end discharge version, the bottom of the rake was ahead and just above the field of view. A summary of the experiment conditions is given in Table 6 and calculated mean speeds over the complete vector field are given in Table 7. *Vx* was defined as flow parallel to the direction of motion of the towing carriage, *Vy* was the vertical flow component and *Vz* was the through plane flow, based on a right-handed coordinate system.

File	δt (μs)	Seeding	Laser power	Carriage speed
Test_05	5000	Rake, side holes	50%	0.1 m/s
Test_06	3000	Rake, side holes	50%	0.3 m/s
Test_07	2000	Rake, side holes	50%	0.5 m/s
Test_08	3000	Rake, side holes	50%	0.5 m/s
Test_09	1000	Rake, side holes	50%	0.75 m/s
Test_10	1000	Rake, side holes	50%	1.00 m/s
Test_23	300	Rake, end hole	50%	0.75 m/s
Test_24	300	Residual	50%	0.75 m/s

Table 6, Summary of experiments carried out in steady flow

An effective wake fraction for the seeding system was defined as *(Vc-Vx)/Vc*, (where *Vc* was the speed of the carriage) and the calculated values for each experiment are given in Table 7. These results showed that the smallest wake was for Test_24, which was made with the residual seeding left in the tank from previous runs. This case showed no measurable difference between the flow speed and the carriage speed. In all other cases, the flow was affected by the presence of the seeding system. For the side-discharge seeding system, at the lowest speed (Test_05), the calculated velocity was within 14% of

the free stream speed, but in all other cases the effective wake fraction was between 25% and 50%. There was a significant reduction in the wake between the side discharge version (Test_09) and the end discharge version (Test_23), but even the end discharge version has a significant effect on the flow.

File	Carriage Speed, m/s	Mean value calculated from PIV, m/s					
	Vc	Vx	Vy	Vz	**|V|**	Rms (**V**)	Wake fraction
Test_05	-0.1	-0.114	0.01	0.008	0.122	0.031	-0.14
Test_06	-0.3	-0.148	0.013	0.037	0.174	0.056	0.507
Test_07	-0.5	-0.244	0.015	0.064	0.299	0.01	0.512
Test_08	-0.5	-0.198	0.02	0.062	0.278	0.166	0.604
Test_09	-0.75	-0.349	0.019	0.107	0.416	0.135	0.535
Test_10	-1	-0.753	-0.008	0.664	1.194	0.471	0.247
Test_23	-0.75	-0.532	0.054	-0.046	0.563	0.082	0.291
Test_24	-0.75	-0.75	0.031	-0.223	0.84	0.184	0

Table 7, Summary of PIV flow measurements, prototype seeding system

Neither of the systems used gave consistently even particle distribution. The side discharge system resulted in periodic waves of particles across the field of view, shown in Figure 9, whereas the end discharge system resulted in periodic clouds of particles, shown in Figure 10. The periodic waves were possibly caused by vortices shed off the rake, whereas the periodic clouds were probably caused by the mixing of the jet from the rake with the undisturbed flow. The end discharge system also resulted in air bubbles appearing in the field of view, which can be seen at the top of Figure 10.

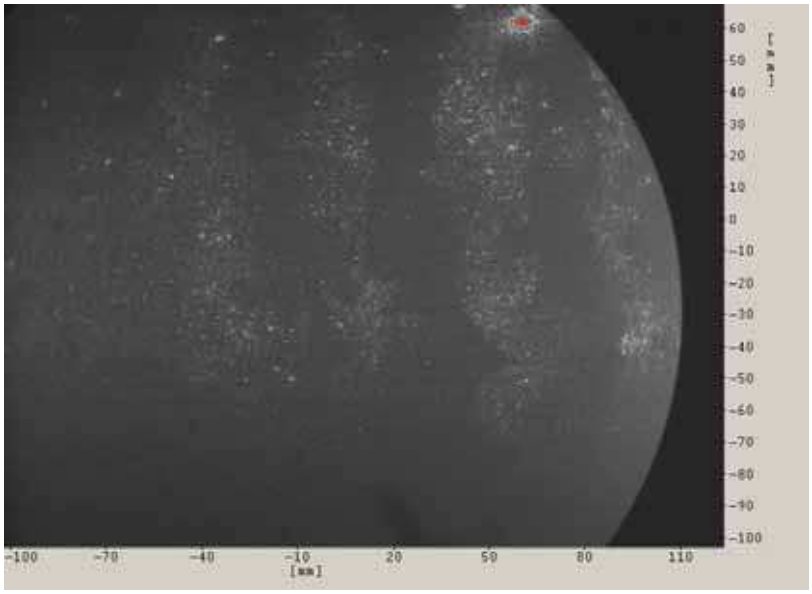

Figure 9, Seeding particles from side discharge rake at 0.75 m/s, showing periodic waves of particles

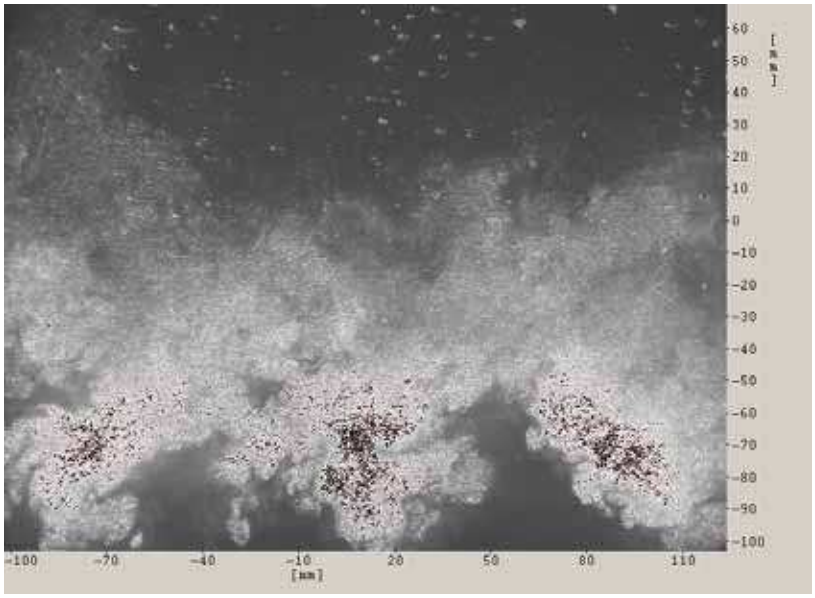

Figure 10, Seeding particles from end discharge rake at 0.75 m/s, showing periodic clouds of particles

SEEDING RAKE DESIGN IMPROVEMENTS

The prototype seeding rake, with side discharge was used for a set of preliminary experiments to measure the flow around an escort tug with a yaw angle (Molyneux and Xu, 2005). These experiments showed that a seeding rake was necessary for measuring flow around a hull with a yaw angle; otherwise there was insufficient seeding concentration in the measurement area, especially on the downstream side of the hull. During the preliminary experiments with the ship model, it was also found that for a

measurement plane orientation across the direction of motion of the carriage, a single discharge pipe gave a narrow band of particles that did not extend across the whole field of view of the cameras. The preliminary experiments had also shown that it was unlikely that one seeding system would be suitable for all measurement locations.

A second generation of seeding system was required, which had improved performance relative to the prototype system. The key features required were an even distribution of particles, and a reduced wake. The revised seeding rakes were constructed from smaller diameter pipe (to reduce the wake) and multiple fingers to extend the width of the particle clouds. Two rakes were made with vertical fingers, one with three fingers and a maximum dimension of 300 mm across the flow and one with five fingers and a maximum dimension of 500 mm across the flow. A second orientation was used with three fingers oriented horizontally, with a maximum dimension of 300 mm across the flow. This orientation was designed for measuring flow under the hull. These rakes are shown in Figures 11 to 13.

All of the rakes were made from copper pipe, with an inside diameter of 12mm. The smaller diameter, relative to the prototype system was used in an attempt to reduce the overall wake of the rake. Each finger had two rows of holes (3 mm diameter on 25 mm spacing). Seeded fluid was injected normal to the direction of motion of the rake.

The wake of the five-fingered rake was determined from experiments in the ice tank at NRC's Institute for Ocean Technology. Two speeds were investigated, 0.5 m/s and 1.0 m/s, which were set from a computer file specified the acceleration rate, the steady speed and the deceleration rate. One file was created for each speed, and only these files were used to control the carriage during the experiments. The steady speed part of the profile was checked against an independent sensor for five runs at each speed. The comparison between the set speed and the independently verified speed is given in Table 8.

The five-fingered seeding rake was used, since it had the largest effective area, which covered the whole of the measurement window of the PIV system. It was fixed with its fingers across the direction of the undisturbed flow and parallel to the laser plane directed across the direction of motion for the carriage. The rake position was moved over the maximum distance that was practically obtainable. Three locations for the rake, with distances of 720 mm, 1400 mm and 3600 mm ahead of the laser sheet. A sketch of the orientation of the seeding rake, the laser sheet and the direction of motion of the fluid is given in Figure 14.

For these experiments, the coordinate system was different from that used with the preliminary seeding system, due to the re-orientation of the laser sheet. *Vx* was defined as flow parallel to the laser sheet, *Vy* was the vertical flow component (positive towards the free surface) and *Vz* was the through the laser plane flow, based on a right-handed coordinate system. *Vc* was the speed of the carriage (assumed to be the same as the undisturbed flow).

Figure 11, Five-fingered vertical seeding rake

Figure 12, Three-fingered vertical seeding rake

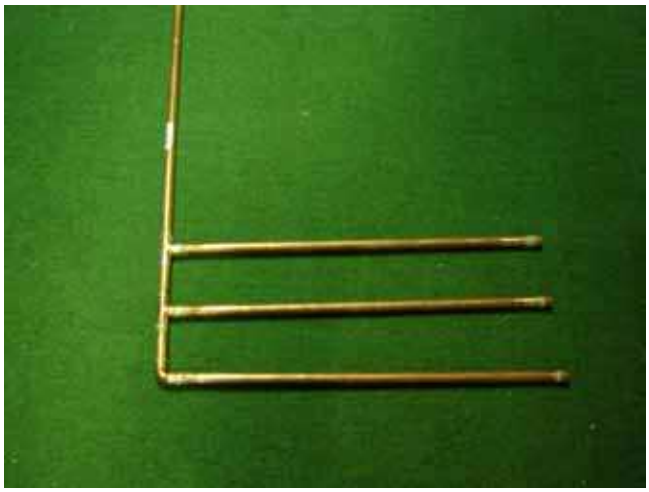

Figure 13, Three-fingered horizontal seeding rake

Nominal value (m/s)			*Vc* m/s		Segment Time sec	Number Samples N
	T1	T2	Mean	Std. Devn.		
0.50	19.28	71.58	0.49971	0.000673	52.3	2615
0.50	24.62	85.42	0.49957	0.000606	60.8	3040
0.50	31.94	90.06	0.49951	0.000556	58.12	2906
0.50	14.78	84.42	0.49962	0.000634	69.64	3482
0.50	14.82	91.94	0.49973	0.000572	77.12	3856
Average value			**0.49963**			
1.00	24.28	55.86	0.99916	0.000759	31.58	1579
1.00	26.22	57.8	0.99919	0.000749	31.58	1579
1.00	23.48	58.3	0.99942	0.000776	34.82	1741
1.00	21.48	57.04	0.99931	0.000751	35.56	1778
1.00	32.82	74.18	0.99952	0.000808	41.36	2068
Average value			**0.99932**			

Table 8, Results of experiments to check carriage speed

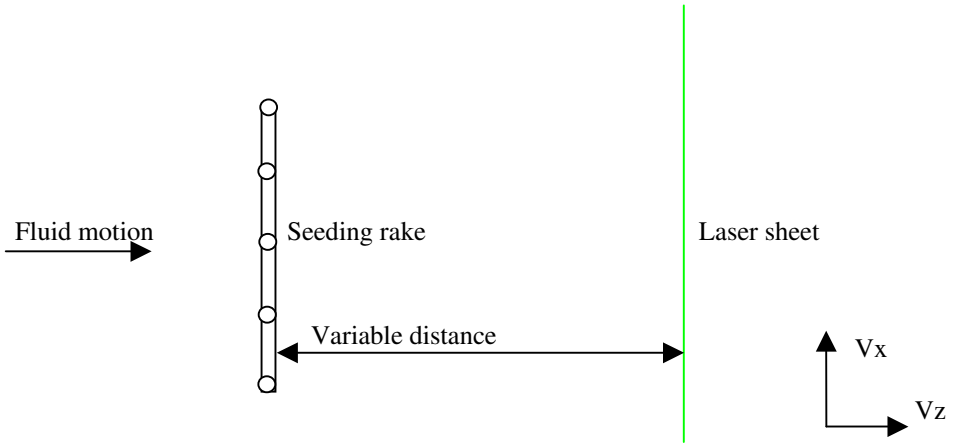

Figure 14, Orientation of seeding rake and laser sheet, and velocity components

For the case with no ship model present, it was possible to pre-seed the fluid and remove the rake during data collection. These experiments were used to confirm the accuracy of the PIV system. In this situation, seeding was carried out when the carriage was going in reverse towards its home point and then removing the rake for the PIV measurements, made with the carriage going forwards.

In all the experiments, determining the optimum time interval between laser exposures required a certain amount of trial and error to obtain flow vectors over the maximum area within the field of view.

The time between individual runs was approximately five minutes, although in some cases it was as low as three and in others it was as high as ten. It was not necessary to let all the particles settle out of the fluid but it was important that the disturbances caused by the passage of the rake had died out, before a new data collection run was started.

All data for this series of experiments was collected and analyzed using DaVis 7.1, an upgraded version of the software used for the experiments with the prototype rakes. The average and RMS deviation were calculated from the 50 pairs of PIV frames, using the time averaging function average function within DaVis 7.1. This function has a threshold value for the minimum number of time steps with a vector at a given interrogation window before the average and RMS values are calculated. For all data sets used in the wake analysis the threshold value was set at 7. Varying this parameter from 5 to 50 produced variations of the mean value of the vector modulus of less than 1.5%. The value of 7 was found to be a reasonable compromise to remove values based on very small numbers of points, without removing significant amounts of information.

The calculated vector components with and without the seeding rake are given in Tables 9 and 10 for speeds of 0.5 m/s and 1.0 m/s respectively. Included in these tables are the results of the experiments with no seeding system.

In all cases it can be seen that the x and y components of the flow (within the measurement plane) are effectively zero, compared to the z velocity component (through the measurement plane).

The results show that at 0.5 m/s the location of the rake has little effect on the measured mean flow. The mean flow was between 10% and 12% lower than the nominal free stream case. The RMS deviation of the flow did not change with the location. At 1 m/s, the average wake fraction based on the three measurement locations was 15% of the free stream flow. There was more variation in the results than at 0.5 m/s, which may have been due to more turbulence in the flow. At 1 m/s, it was noticeable that the RMS deviation of the velocity decreased as the distance from the rake increased, whereas for 0.5 m/s it was approximately constant. In both cases where the seeding rake was removed, the free stream speed calculated by the PIV system was the same as the set speed (within 95% Confidence Interval).

Rake at 720 mm away from laser				δt, μs
Cam_Date=060201_Time=095416				1000
	min	max	mean	rms
Vx	-0.10506	0.15533	0.00203	0.02156
Vy	0.08426	-0.09290	-0.00246	0.01382
Vz	0.34589	0.55785	0.43743	0.02119
/V/	0.34935	0.57509	0.43818	0.02132
Vc			0.49963	
Wake fraction			0.124498	

Rake @ 1400mm away from laser				δt, μs
Cam_Date=060131_Time=161447				500
	min	max	mean	rms
Vx	-0.22546	0.29304	0.00536	0.03306
Vy	0.26403	-0.23092	-0.00643	0.02351
Vz	0.21475	0.63912	0.43851	0.02723
/V/	0.23608	0.69629	0.44036	0.02890
Vc			0.49963	
Wake fraction			0.122329	

Rake at 3600 mm away from laser				δt, μs
Cam_Date=060201_Time=103347				1000
	min	max	mean	rms
Vx	-0.14252	0.11699	-0.00139	0.01977
Vy	0.13939	-0.13122	-0.00145	0.01467
Vz	0.36573	0.55456	0.45032	0.01851
/V/	0.36672	0.55622	0.45097	0.01912
Vc			0.49963	
Wake fraction			0.098695	

No seeding rake				δt, μs
Cam_Date=060201_Time=104950				500
	min	max	mean	rms
Vx	-0.17004	0.28746	0.01635	0.02688
Vy	0.20805	-0.15970	-0.00591	0.02486
Vz	0.24920	0.67043	0.50790	0.02547
/V/	0.38104	0.68193	0.50951	0.02545
Vc			0.49963	
Wake fraction			-0.01655	

Table 9, Results from experiments at nominal speed of 0.5 m/s

Rake at 720 mm away from laser				δt, μs
Cam_Date=060201_Time=100604				500
	min	max	mean	rms
Vx	-0.35342	0.36902	0.01803	0.05916
Vy	0.26067	0.24988	-0.01902	0.03675
Vz	0.61718	1.30182	0.87445	0.07062
/V/	0.64439	1.30560	0.87747	0.07233

Vc	0.99932
Wake fraction	0.124955

Rake @ 1400mm away from laser				δt, μs
Cam_Date=060131_Time=163013				700
	min	max	mean	rms
Vx	-0.20548	0.21266	-0.00401	0.03873
Vy	0.12146	-0.16017	-0.00924	0.02317
Vz	0.69619	0.96175	0.81102	0.04233
/V/	0.69984	0.98357	0.81232	0.04281

Vc	0.99932
Wake fraction	0.188427

Rake at 3600 mm away from laser				δt, μs
Cam_Date=060201_Time=104155				700
	min	max	mean	rms
Vx	-0.20670	0.23962	0.01007	0.03318
Vy	0.13346	-0.11231	-0.00091	0.02102
Vz	0.72836	1.02592	0.85856	0.03355
/V/	0.75712	1.03112	0.85950	0.03396

Vc	0.99932
Wake fraction	0.140855

No seeding rake				δt, μs
Cam_Date=060201_Time=105457				500
	min	max	mean	rms
Vx	-0.16372	0.25600	0.00659	0.03708
Vy	0.20408	-0.18448	-0.01302	0.02740
Vz	0.88357	1.20391	0.98504	0.04024
/V/	0.84217	1.20609	0.98622	0.04045

Vc	0.99932
Wake fraction	0.014289

Table 10, Results from experiments at nominal speed of 1.0 m/s

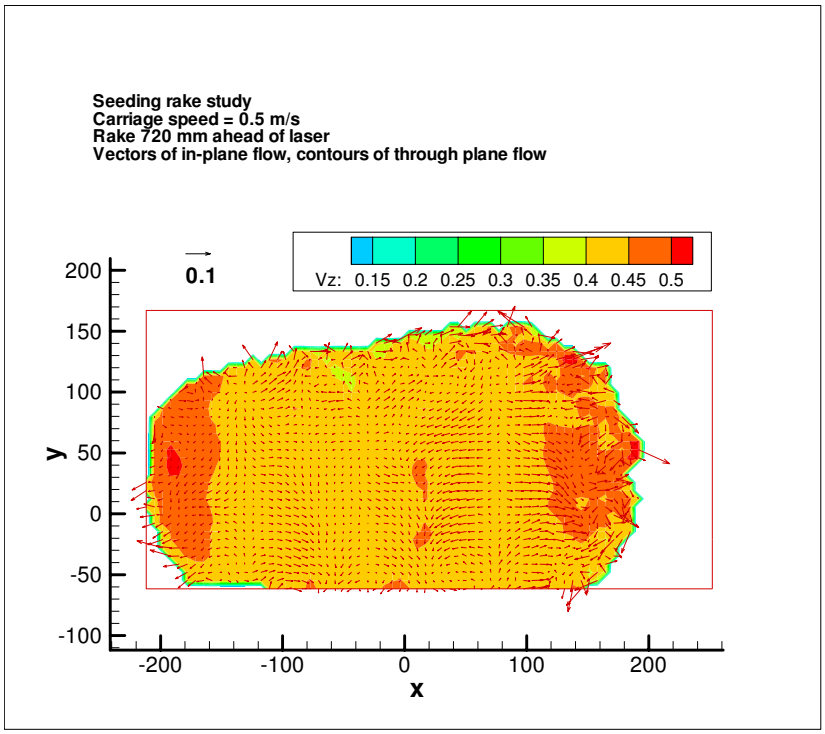

Figure 15, Calculated flow patterns for 0.5 m/s, rake at 720 mm ahead of laser

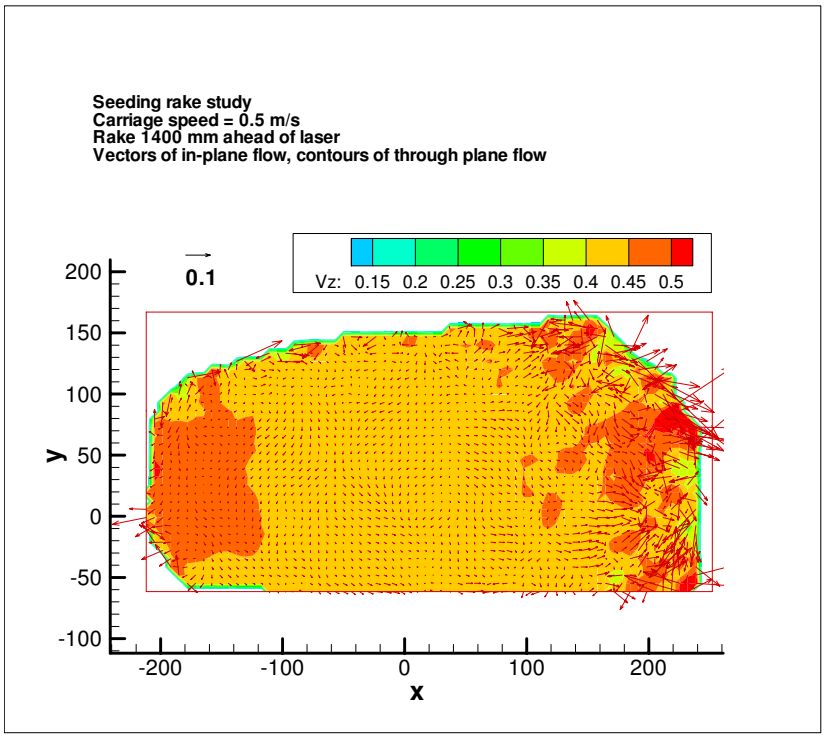

Figure 16, Calculated flow patterns for 0.5 m/s, rake at 1400 mm ahead of laser

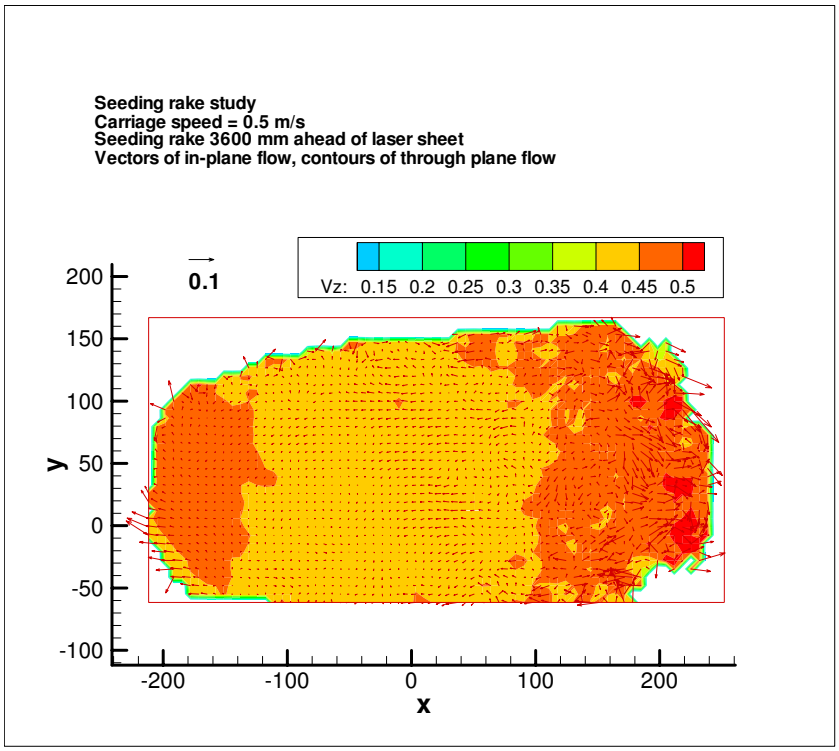

Figure 17, Calculated flow patterns for 0.5 m/s, rake at 3600 mm ahead of laser

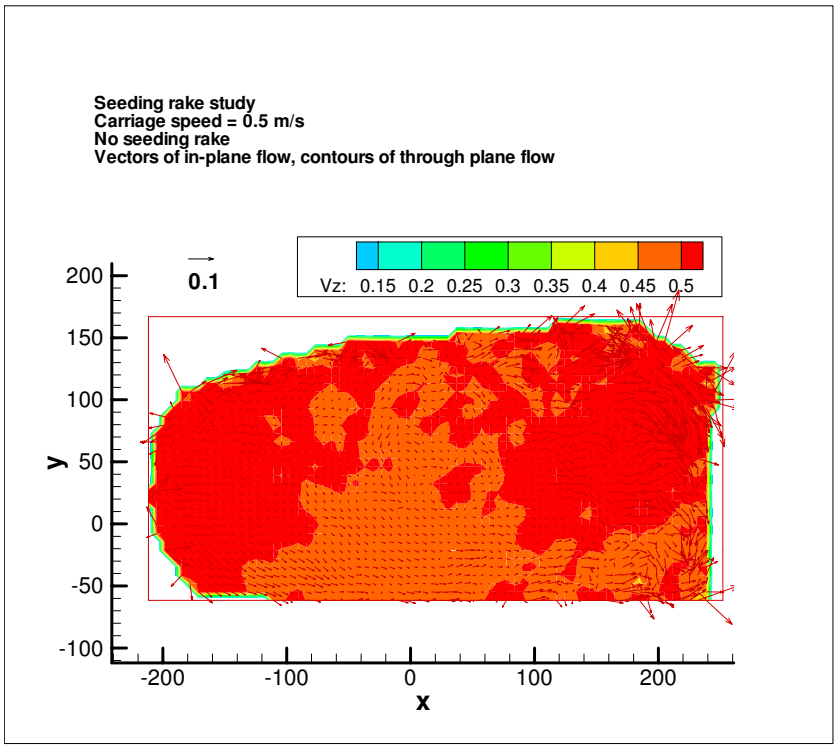

Figure 18, Calculated flow patterns for 0.5 m/s, no seeding rake

Close to the seeding rake, the wake from the individual fingers could be seen as vertical bands within the in-plane plane velocity vectors. This pattern dissipated as the distance from the rake increased. This is illustrated in Figures 15 to 17, which show flow measurements for 0.5 m/s, for the seeding rake at distances of 720 mm 1400mm and 3600 mm from the laser sheet. The case with no seeding rake is shown in Figure 18.

When the seeding rake was removed, the number of vectors used to calculate the mean flow pattern was smaller than for the cases with active seeding. This highlights that even for very steady flow, the seeding rake provides uniform seeding concentration, but the average flow speed behind the rake is 12 to 15% lower than the nominal free stream case. It is hoped that by having a seeding rake that extends beyond the measurement region of the PIV system, that all the flow through the measurement window will be slowed by a uniform amount. Flow patterns around an object, such as a ship model with different geometries, should be comparable, if the same seeding rake and approximate location are used for both sets of experiments.

The new seeding rake creates a more even distribution of particles than the prototypes. Figure 19 shows a particle image taken at 0.5 m/s with the laser 1400mm behind the seeding rake. This figure does not show the periodic waves of particles shown in Figure 7 or the clouds of particles shown in Figure 8. The calculated flow patterns for the particles shown in Figure 19 are given in Figure 16.

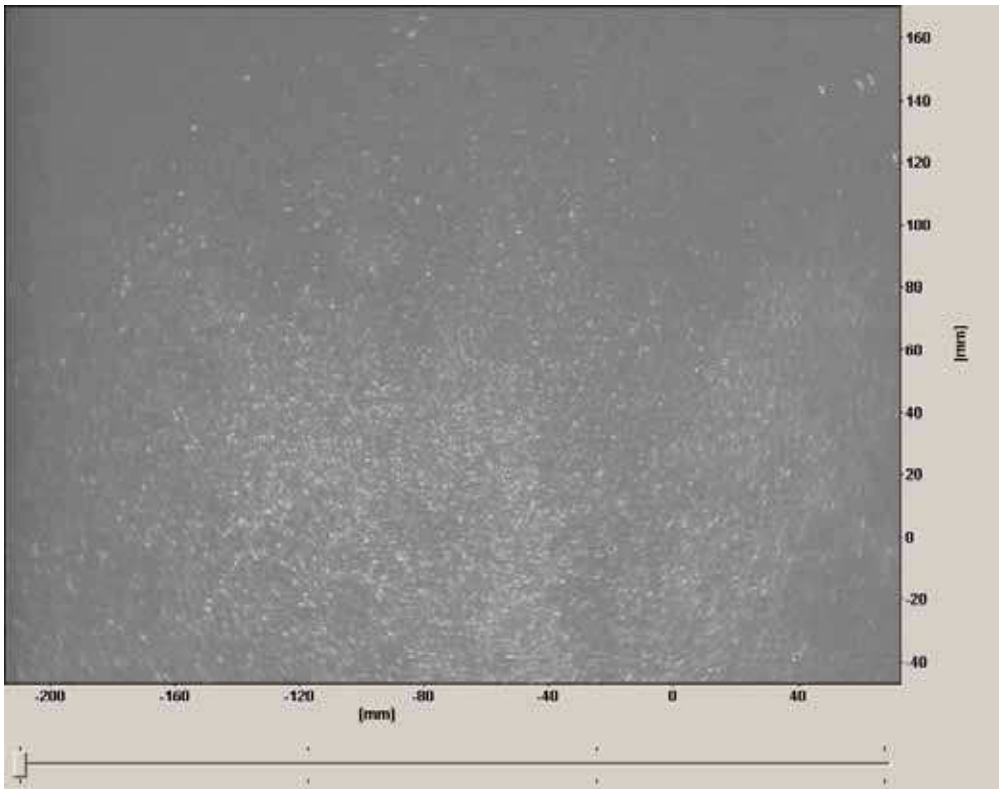

Figure 19, Particle distribution behind the seeding rake, 0.5 m/s

CONCLUSIONS

A preliminary study (Molyneux and Xu, 2005) had shown that it was necessary to use a seeding rake when carrying out experiments using PIV to measure the flow vectors around a ship model in a towing tank. Without active seeding of the flow, it was not possible to make consistent measurements of flow velocity, especially on the downstream side of the hull, because the seed particle concentration was too low. The rake was needed to deliver seeding particles into the flow, and maintain the minimum concentration required for accurate measurements. Ideally the rake should have no effect on the flow, but this is impossible. The next best option is to have minimum disturbance to the flow, and to have that disturbance distributed uniformly across the measurement window of the PIV system.

The rakes used for these experiments create a uniform disturbance across the measurement area, but reduced the mean flow speed by 12 to 15%, depending on the flow speed. The location of the rake relative to the measurement area has little effect on the measured mean speed, but the particle concentration decreases as the distance is increased. Since the area of the rake is large, in relation to the measurement area, it should affect all of the flow being studied. As a result, if the same rake and relative location are used, then flow patterns measured for different geometric arrangements of a ship model should be comparable, but with a similar bias to the results, caused by the presence of the seeding rake.

The estimated uncertainty for the PIV velocity analysis is within the range discussed by other researchers, and is expected to be between 8% and 16%. The 8% values of uncertainty are estimated for a flow speed of 1.0 m/s with laser pulse times of 1000 μs. The 16% value of uncertainty was estimated for a flow speed of 0.5 m/s, with a laser pulse time of 500 μs.

Using a smaller measurement area, with less magnification, would lower the uncertainty. Another way of lowering the uncertainty would be to increase the time between the laser pulses. The nature of the expected flow patterns for the escort tug required the relatively high uncertainty to be accepted for two main reasons. The first was the desire for a large measurement area to maximize the data collected in unsteady flow conditions from a single field of view. The second requirement was for the measurement plane across the strongest flow direction, since this is the primary plane of interest for many flow measurements around a ship hull (e.g. a wake survey through the propeller plane). This required relatively short laser pulse times to ensure the same particles are within the measurement space for both image pairs.

ACKNOWLEDGEMENTS

I wish to thank the following people. Professor Neil Bose, Canada Research Chair in Offshore and Underwater Vehicles Design at Memorial University, is thanked for his continuing support and encouragement of our efforts to understand PIV and develop it into a practical experiment technique for ocean engineering and naval architecture research. Ms. Jie Xu is thanked for her leadership, continuous dedication and attention to detail that is necessary for making successful PIV experiments. Mr. Jim Gosse, Laboratory Technician in the Fluids Laboratory at Memorial University is thanked for all his help during the set-up and carrying out the experiments in the OERC Towing Tank at MUN. Finally, I wish to thank the staff at IOT for preparing the model for testing and assisting with the many tasks required during experiments at IOT.

REFERENCES

Calagno, G., Di Felice, F., Felli, M, and Pereira, F. 2002 'Application of Stereo PIV: Propeller Wake Analysis in a Large Circulating Water Channel', 11th Symposium on Applications of Laser Techniques to Fluid Mechanics, Calouste Gulbenkian Foundation, Lisbon, Portugal, 8th to 11th July, Paper 26-4.

Di Felice, F. & De Gregorio, F. 2000 'Ship Model Wake Analysis by Means of PIV in a Large Circulating Water Channel', Proceedings of 10th International Offshore and Polar Engineering Conference, Seattle, USA, May 28-June 2, pp. 392-397

Gui, L., Longo, J. and Stern, F. 2001, 'Towing Tank PIV Measurement System, Data and Uncertainty Assessment for DTMB Model 5512', *Experiments in Fluids*, Volume 31, pp. 336-346.

LaVision GmbH, 2005 'DaVis FlowMaster Software Manual for DaVis 7.0', June 8.

LaVision GmbH, 2004 'DaVis Software Manual for DaVis 6.2', January.

Lawson, N. J. and Wu, J. 1997a 'Three-dimensional Particle Image Velocimetry: Error Analysis of Stereoscopic Techniques', *Measurement Science and Technology*, Volume 8, pp 894-900.

Lawson, N. J. and Wu, J. 1997b 'Three-dimensional Particle Image Velocimetry: Experimental Error Analysis of a Digital Angular Stereoscopic System', *Measurement Science and Technology*, Volume 8, pp 1455-1464.

Molyneux, D. and Xu, J. 2005 'Particle Image Velocimetry Experiments to Measure Flow Around an Escort Tug', IOT/NRC, TR-2005-10.

Potters Industries Inc 2005 Product Specification Sheet, http://www.pottersbeads.com/literature/SC_Hollow_Glass_Spheres.pdf, May.

Soloff, S. M., Adrian, R. J. and Liu, Z-C. 1997 'Distortion Compensation for Generalized Stereoscopic Particle Image Velocimetry', *Measurement Science and Technology*, Volume 8, pp 1441-1454.

Xu, J., Molyneux, D. and Bose, N. 2005 'A Versatile Particle Image Velocimetry System for Flow Measurements in Water Tanks', 7th Canadian Marine Hydromechanics and Structures Conference, Halifax, N. S. September.